About The Cover

COVER Crystal structure of the 80*S* ribosome from the yeast *Saccharomyces cerevisiae*. Ribosomes are responsible for protein synthesis in all cells. The eukaryotic ribosome, which consists of four RNA chains (gray) and 79 different proteins (colored ribbons), is more intricate and 40% larger than its bacterial counterpart. With an atomic mass of 3.3 megadaltons, this is the largest asymmetrical structure resolved by x-ray crystallography to date. See page 1524.
Image: Sergey Melnikov, Nicolas Garreau de Loubresse, Adam Ben-Shem, Lasse Jenner, Gulnara Yusupova, Marat Yusupov/Institut de Génétique et de Biologie Moléculaire et Cellulaire, Université de Strasbourg

therefore represent promising directions for future study.

Conclusion. Given the ever-growing, technology-driven data stream in today's scientific world, there is an increasing need for tools to make sense of complex data sets in diverse fields. The ability to examine all potentially interesting relationships in a data set—independent of their form—allows tremendous versatility in the search for meaningful insights. On the basis of our tests, MINE is useful for identifying and characterizing structure in data.

References and Notes

1. T. Hastie, R. Tibshirani, J. H. Friedman, *The Elements of Statistical Learning: Data Mining, Inference, and Prediction* (Springer Verlag, New York, 2009).
2. Science Staff, *Science* **331**, 692 (2011).
3. By "functional relationship" we mean a distribution (X,Y) in which Y is a function of X, potentially with independent noise added.
4. A. Caspi *et al*., *Science* **301**, 386 (2003).
5. R. N. Clayton, T. K. Mayeda, *Geochim. Cosmochim. Acta* **60**, 1999 (1996).
6. T. J. Algeo, T. W. Lyons, *Paleoceanography* **21**, PA1016 (2006).
7. World Health Organization Statistical Information Systems, *World Health Organization Statistical Information Systems (WHOSIS)* (2009); www.who.int/whosis/en/.
8. A. Rényi, *Acta Math. Hung.* **10**, 441 (1959).
9. C. J. Stone, *Ann. Stat.* **5**, 595 (1977).
10. W. S. Cleveland, S. J. Devlin, *J. Am. Stat. Assoc.* **83**, 596 (1988).
11. For both splines and regression estimators, we used R^2 with respect to the estimated spline/regression function to score relationships.
12. Y. I. Moon, B. Rajagopalan, U. Lall, *Phys. Rev. E Stat. Phys. Plasmas Fluids Relat. Interdiscip. Topics* **52**, 2318 (1995).
13. G. Darbellay, I. Vajda, *IEEE Trans. Inf. Theory* **45**, 1315 (1999).
14. A. Kraskov, H. Stögbauer, P. Grassberger, *Phys. Rev. E Stat. Nonlin. Soft Matter Phys.* **69**, 066138 (2004).
15. L. Breiman, J. H. Friedman, *J. Am. Stat. Assoc.* **80**, 580 (1985).
16. T. Hastie, W. Stuetzle, *J. Am. Stat. Assoc.* **84**, 502 (1989).
17. R. Tibshirani, *Stat. Comput.* **2**, 183 (1992).
18. B. Kégl, A. Krzyzak, T. Linder, K. Zeger, *Adv. Neural Inf. Process. Syst.* **11**, 501 (1999).
19. P. Delicado, M. Smrekar, *Stat. Comput.* **19**, 255 (2009).
20. "Principal curve-based methods" refers to mean-squared error relative to the principal curve, and CorGC, the principal curve-based measure of dependence of Delicado *et al*.
21. G. Székely, M. Rizzo, *Ann. Appl. Stat.* **3**, 1236 (2009).
22. B. P. Tu, A. Kudlicki, M. Rowicka, S. L. McKnight, *Science* **310**, 1152 (2005).
23. R. Fisher, Tests of significance in harmonic analysis. *Proc. R. Soc. Lond. A* **125**, 54 (1929).
24. M. Ahdesmäki, H. Lähdesmäki, R. Pearson, H. Huttunen, O. Yli-Harja, *BMC Bioinformatics* **6**, 117 (2005).
25. H. Rosling, Gapminder, *Indicators in Gapminder World* (2008); www.gapminder.org/data/
26. P. T. Spellman *et al*., *Mol. Biol. Cell* **9**, 3273 (1998).
27. Baseball Prospectus Statistics Reports (2009); www.baseballprospectus.com/sortable/
28. S. Lahman, The Baseball Archive, *The Baseball Archive* (2009); baseball1.com/statistics/
29. P. J. Turnbaugh *et al.*, The effect of diet on the human gut microbiome: A metagenomic analysis in humanized gnotobiotic mice. *Sci. Transl. Med.* **1**, 6ra14 (2009).
30. L. Chen *et al*., *Lancet* **364**, 1984 (2004).
31. S. Desai, S. Alva, *Demography* **35**, 71 (1998).
32. S. Gupta, M. Verhoeven, *J. Policy Model.* **23**, 433 (2001).
33. T. Gill *et al*., Obesity in the Pacific: Too big to ignore. *Noumea, New Caledonia: World Health Organization Regional Office for the Western Pacific, Secretariat of the Pacific Community* (2002).
34. RPMLV estimates how many more runs per game a player contributes over a replacement-level player in an average lineup.
35. P. J. Turnbaugh *et al*., *Nature* **449**, 804 (2007).
36. R. E. Ley *et al*., *Science* **320**, 1647 (2008).
37. *The World Factbook 2009* (Central Intelligence Agency, Washington, DC, 2009).

Acknowledgments: We thank C. Blättler, B. Eidelson, M. D. Finucane, M. M. Finucane, M. Fujihara, T. Gingrich, E. Goldstein, R. Gupta, R. Hahne, T. Jaakkola, N. Laird, M. Lipsitch, S. Manber, G. Nicholls, A. Papageorge, N. Patterson, E. Phelan, J.Rinn, B. Ripley, I. Shylakhter, and R. Tibshirani for invaluable support and critical discussions throughout; and O. Derby, M. Fitzgerald, S. Hart, M. Huang, E. Karlsson, S. Schaffner, C. Edwards, and D. Yamins for assistance. P.C.S. and this work are supported by the Packard Foundation. For data set analysis, P.C.S. was also supported by NIH MIDAS award U54GM088558, D.N.R. by a Marshall Scholarship, M.M. by NSF grant 0915922, H.K.F. by ERC grant 239985, S.R.G. by the Medical Scientist Training Program, and P.J.T. by NIH P50 GM068763. Data and software are available online at http://exploredata.net.

Supporting Online Material

www.sciencemag.org/cgi/content/full/334/6062/1518/DC1
Materials and Methods
SOM Text
Figs. S1 to S13
Tables S1 to S14
References (*38*–*54*)

10 March 2011; accepted 5 October 2011
10.1126/science.1205438

The Structure of the Eukaryotic Ribosome at 3.0 Å Resolution

Adam Ben-Shem,*† Nicolas Garreau de Loubresse,* Sergey Melnikov,* Lasse Jenner, Gulnara Yusupova, Marat Yusupov†

Ribosomes translate genetic information encoded by messenger RNA into proteins. Many aspects of translation and its regulation are specific to eukaryotes, whose ribosomes are much larger and intricate than their bacterial counterparts. We report the crystal structure of the 80*S* ribosome from the yeast *Saccharomyces cerevisiae*—including nearly all ribosomal RNA bases and protein side chains as well as an additional protein, Stm1—at a resolution of 3.0 angstroms. This atomic model reveals the architecture of eukaryote-specific elements and their interaction with the universally conserved core, and describes all eukaryote-specific bridges between the two ribosomal subunits. It forms the structural framework for the design and analysis of experiments that explore the eukaryotic translation apparatus and the evolutionary forces that shaped it.

Ribosomes are responsible for the synthesis of proteins across all kingdoms of life. The core, which is universally conserved and was described in detail by structures of prokaryotic ribosomes, catalyzes peptide bond formation and decodes mRNA (*1*). However, eukaryotes and prokaryotes differ markedly in other translation processes such as initiation, termination, and regulation (*2*, *3*), and eukaryotic ribosomes play a central role in many eukaryote-specific cellular processes. Accordingly, eukaryotic ribosomes are at least 40% larger than their bacterial counterparts as a result of additional ribosomal RNA (rRNA) elements called expansion segments (ESs) and extra protein moieties (*4*).

All ribosomes are composed of two subunits. The large 60*S* subunit of the eukaryotic ribosome (50*S* in bacteria) consists of three rRNA molecules (25*S*, 5.8*S*, and 5*S*) and 46 proteins, whereas the small 40*S* subunit (30*S* in bacteria) includes one rRNA chain (18*S*) and 33 proteins. Of the 79 proteins, 32 have no homologs in crystal structures of bacterial or archaeal ribosomes, and those that do have homologs can still harbor large eukaryote-specific extensions (*5*). Apart from variability in certain rRNA expansion segments, all eukaryotic ribosomes, from yeast to human, are very similar.

Three-dimensional cryoelectron microscopy (cryo-EM) reconstructions of eukaryotic ribosomes at 15 to 5.5 Å resolution provided insight into the interactions of the ribosome with several factors (*4*, *6*–*8*). A crystal structure of the *S. cerevisiae* ribosome at 4.15 Å resolution described the fold of all ordered rRNA expansion segments, but the relatively low resolution precluded localization of most eukaryote-specific proteins (*9*). Crystallographic data at a better resolution (3.9 Å) from the *Tetrahymena thermophila* 40*S* led to a definition of the locations and folds of all eukaryote-specific proteins in the

Institut de Génétique et de Biologie Moléculaire et Cellulaire, 1 rue Laurent Fries, BP10142, Illkirch F-67400, France; INSERM, U964, Illkirch F-67400, France; CNRS, UMR7104, Illkirch F-67400, France; and Université de Strasbourg, Strasbourg F-67000, France.

*These authors contributed equally to this work.
†To whom correspondence should be addressed. E-mail: adam@igbmc.fr (A.B.-S.); marat@igbmc.fr (M.Y.)

small subunit (*10*). However, an atomic model of the full eukaryotic ribosome is lacking. We report here the complete structure of the 80*S* ribosome from *S. cerevisiae* at a resolution of 3.0 Å.

Structure determination and content. Earlier, we presented a lower-resolution model that was based on x-ray data from a single crystal (*9*). To extend the resolution of the electron density maps, we collected data from 13 isomorphous crystals (*11*). Improvements in crystal treatment and data collection methodology were also instrumental in obtaining a full data set at 3.0 Å resolution (*11*) (table S1). Phases obtained from the refined lower-resolution model were combined with experimental single-wavelength anomalous dispersion (SAD) phases derived from ~1400 osmium hexamine sites. The last round of model refinement gave R_{free}/R_{work} = 22.8%/18.2%. The final model consists of two ribosomes in the asymmetric unit, termed ribosome A and B, that differ markedly in the degree of rotation of 40*S* relative to 60*S* (4° in A, 9° in B) and the extent of 40*S* head swiveling (15.5° in A, 10.5° in B).

Ordered protein side chains were clearly visible in the electron density maps, and it was possible in most cases to distinguish between rRNA purines and pyrimidines (fig. S1). Mass spectrometry analysis identified Stm1 as the only nonribosomal component in our ribosome preparations, and residues 9 to 176 of this protein could be traced. The final model contains all 44 proteins that are absent in bacteria and all 35 universally conserved proteins, with the exception of the highly mobile L1, regions within the P-stalk proteins, and residues located in disordered loops or tails (Fig. 1 and table S2). The rRNA is modeled almost completely, except for the major hairpin of ES27L, part of the L1 stalk, and a small part of ES7L (Fig. 1 and tables S2 and S3). On the whole, the model includes ~90.5% of all ~13,000 ribosomal protein residues and 95.5% of ~5500 rRNA residues. About 2000 metal ions are also present. To facilitate comparison between ribosomes from different species, we use a simplified ribosomal protein nomenclature based on the names of protein families (table S4).

Overall view of the 80*S* ribosome. An evolutionarily conserved core of the ribosome can be structurally defined by comparing the yeast 80*S* model to its bacterial counterparts (Fig. 2A and figs. S2 to S4) (*12*). The vast majority of the ~1.35 MD of eukaryote-specific parts (350 kD of rRNA expansion segments, 800 kD of proteins absent in bacteria, and 200 kD of eukaryote-specific domains within conserved proteins) are located on the surface of the ribosome, enveloping the evolutionarily conserved core (Fig. 2 and figs. S4 to S6). The largest "patches" on the surface that are relatively poor in eukaryotic elements, although not completely devoid of them, are regions involved in core ribosomal functions at the G protein–binding platform, the rim of the peptide exit tunnel on 60*S* and around the mRNA entry site on 40*S* (Fig. 2).

The two subunits differ markedly in the spatial distribution of rRNA expansion segments and eukaryote-specific proteins. In the small subunit, most eukaryote-specific rRNA is concentrated at the bottom where the two largest expansion segments, ES3S and ES6S, strongly interact. On the other hand, the eukaryote-specific proteins in this subunit are scattered all over its surface, so there is only a weak correlation between the location of rRNA expansion segments and that of eukaryote-specific protein elements (*10*) (Fig. 2B).

By contrast, in 60*S* the numerous expansion segments form a nearly continuous ring that encircles the peptide exit tunnel and stretches from the P-stalk side of the back to its L1 side. Most eukaryote-specific proteins are associated with elements of this ring, and their spatial distribution has the same ring-like feature (Fig. 2B). Comparison of 60*S* to the archaeal large subunit instead of the bacterial one (figs. S7 and S8) leads to similar conclusions.

Many of the eukaryote-specific extensions to the conserved core proteins interact with the rRNA expansion segments in the ring and serve to structurally connect the ring to the core. Interactions between eukaryote-specific moieties on the surface and those extending from the functional centers might facilitate allosteric signal transmission to regulate translation. The conserved proteins that are associated with the polypeptide exit tunnel—L22, L4, L23, and L29—are a striking example (*13*). These proteins contain long extensions, up to 140 Å in the case of L4, that reach the periphery of 60*S* (Fig. 3A).

Abundance of nonhelical elements in rRNA expansion segments. In prokaryotes, RNA helices are linked by regular double-stranded extensions of neighboring helices (*14*, *15*). In contrast, our structure reveals that long linkers within several expansion segments form nonhelical elements. Most of these elements are single-stranded stretches that play a dominant role in the association of

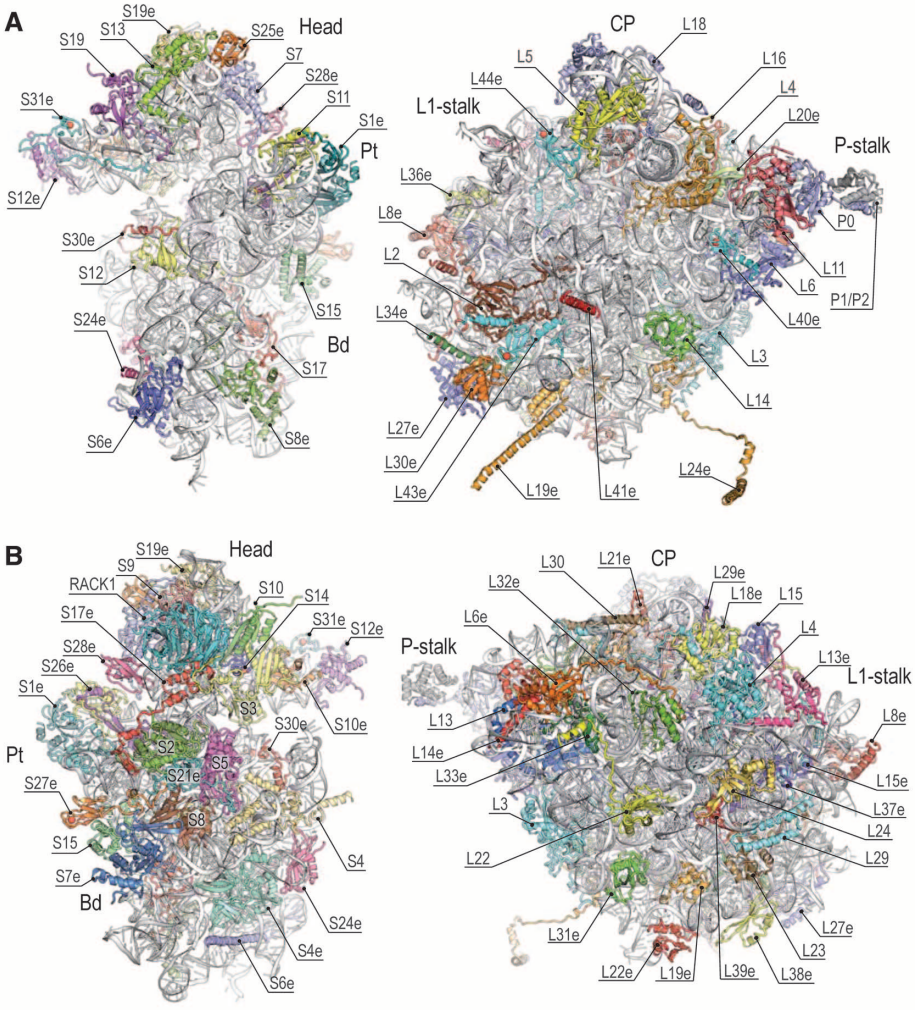

Fig. 1. Architecture of the 80*S* ribosome. (**A**) Interface or "front" view of the 60*S* subunit (left) and 40*S* subunit (right). Landmarks include head, body (Bd), and platform (Pt) of 40*S* as well as central protuberance (CP), L1 stalk, and P stalk of 60*S*. (**B**) Solvent-side or "back" view of the 60*S* and 40*S* subunits.

rRNA expansion segments with proteins (Fig. 3, B and C). Multiple interactions with several proteins, using different binding modes, can be packed within a short single-stranded stretch, as exemplified by a fragment of ES39L (Fig. 3C). The application of such stretches as a platform for protein binding is reminiscent of the assembly of Sm proteins onto the single-stranded Sm-site RNA in spliceosome small nuclear ribonucleoproteins (snRNPs) (*16*).

Eukaryote-specific clusters. Most eukaryote-specific elements on 60*S* can be divided among three areas along the ring: at the back of the P and L1 stalks and around the central protuberance (CP) (Fig. 2B). These areas, together with the ES6S-ES3S cluster on 40*S*, represent the largest concentrations of eukaryote-specific elements. Comparing our yeast 40*S* structure to the one from *T. thermophila* reveals only minor, mostly species-specific, differences in rRNA structure and protein fold (*10*). Therefore, as the small subunit ES6S-ES3S cluster was previously described (*9*, *10*), we focus here on the three 60*S* clusters.

Concentration of eukaryotic elements at the back of the P stalk. ES39L emerges from the back of the large subunit at the P-stalk side (Fig. 2B and Fig. 4A) where, together with a eukaryote-specific α helix in L3, it forms one of the contact sites for the signal recognition particle that targets ribosomes to the endoplasmic reticulum membrane (*17*). The three rRNA helices that constitute ES39L are linked by three stretches of single-stranded rRNA that provide a platform for binding several proteins. The contact between ES39L and its neighboring expansion segment ES7L is mediated by an A-minor interaction where the adenosine stack is donated by ES39L, thereby supporting the idea that the A-minor motif indicates the relative age of its components (fig. S9) (*18*, *19*).

The long bent helix of ES7L encircles L14e and forms extensive interactions with eukaryote-specific proteins and with extensions in conserved proteins (Fig. 4A). The tip of the ES7L helix lies in close proximity to and probably interacts with protein P0, a part of the P stalk that participates in recruiting G proteins to the ribosome (*20*).

Additional binding partners of ES39L include two core proteins, L3 and L6, with domains in proximity to the sarcin-ricin loop (fig. S10)—an element important in the association of G proteins with ribosomes. Furthermore, L3 plays a role in coordinating the processes of accommodating the aminoacyl-tRNA in the peptidyl-transferase center (PTC) (*21*), and L6 lines the binding pocket for eukaryotic elongation factor 2 (eEF2;EF-G in bacteria) (*22*). Thus, ES39L links to functional centers of the ribosome.

Interactions of L6 with protein L14e illustrate a recurrent theme in the yeast ribosome: binding of eukaryote-specific protein elements to conserved ones through interprotein shared β sheets (Fig. 4B). Because these interactions are mediated by the backbones of the two proteins, they pose weak constraints on the sequence of the new element.

Concentration of eukaryotic elements at the back of the L1 stalk. A cluster of four rRNA expansion segments—ES20L, ES26L, ES19L, and ES31L—is located at the back of the L1 stalk (Fig. 2B and Fig. 4C). Both ES20L and ES26L contain a long, narrow, strongly bent loop. The two loops run parallel to one another, forming multiple noncanonical base pairs and stacking interactions (fig. S11). ES31L, which occupies a central position in the cluster, is located opposite the 40*S* mRNA exit site and forms part of the intersubunit bridge eB8. It is physically anchored to the base of the L1 stalk, a mobile element that plays a role in evacuating the exit-site tRNA (*23*), and this connection is reinforced via the C-terminal helix of L8e (Fig. 4C). ES31L contains two helices separated by a rRNA single-stranded stretch, 10 residues in length, that serves as a platform for protein-RNA interactions (Fig. 4, C and D). The cluster of expansion segments harbors several eukaryote-specific proteins as well as the eukaryotic extension of core protein L23, a major component of the "universal docking site" for factors involved in cotranslational targeting, processing, and folding of the nascent chain (Fig. 4C and fig. S12).

Enhanced central protuberance. The CP, dominated by 5*S* rRNA and its surrounding proteins, establishes the conserved physical contacts, or bridges, between the large subunit and the head of the small subunit. These contacts undergo the most drastic rearrangement during the rotation of the small subunit and swiveling of its head (*9*). Because the CP also interacts with functional sites on the large subunit, a role in coordinating the activities on the two subunits was proposed (*9*, *24*, *25*). In eukaryotes, the CP has several additional elements, and its network of interactions with functional sites on the large subunit is considerably expanded (Fig. 4, E and F). An important contribution to this network is due to protein L20e, which forms a junction where multiple RNA elements, including the dynamic P stalk and 5*S*, and several different proteins meet. The seven proteins that

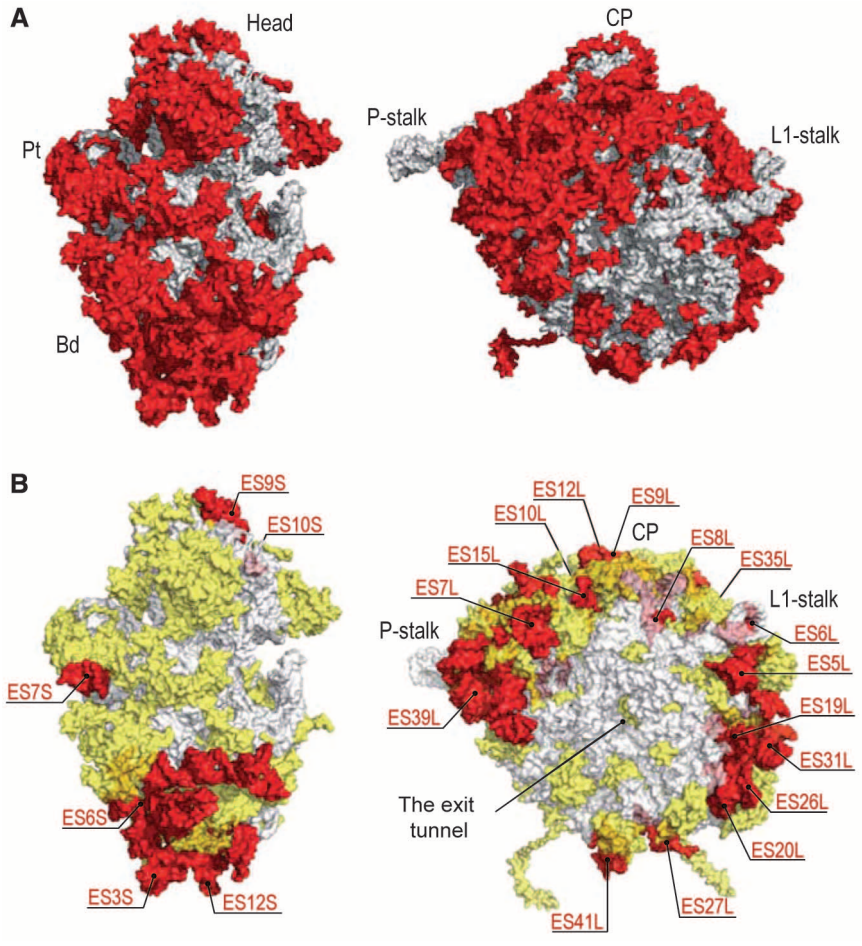

Fig. 2. Characteristics of the 80*S* ribosome surface. (**A**) Abundance of eukaryote-specific elements (in red) on the solvent-side of both subunits. Conserved core elements are in gray. Most of the ribosome surface is eukaryote-specific. (**B**) Distribution of eukaryote-specific protein moieties (yellow) and rRNA expansion segments (red) around the conserved core (gray). Views are of 40*S* from the back and of 60*S* from the back through the peptide exit tunnel. Protein moieties are represented by semitransparent surfaces so that all rRNA expansion segments can be seen.

bind L20e include components of core functional centers that are located far apart (Fig. 4, A and E).

The main rRNA additions to the CP are due to ES9L, which consists of two coaxially stacked helices (partially present in archaea) and to ES12L, which emerges from the base of H38 (Fig. 4E). These elements run parallel to 5*S* rRNA and squeeze between them the C-terminal helix of the eukaryote-specific protein L29e, whose N-terminal domain wiggles through the rRNA core to reach the vicinity of the PTC and the base of H89.

Eukaryote-specific bridges. The contact points between the two subunits play an important

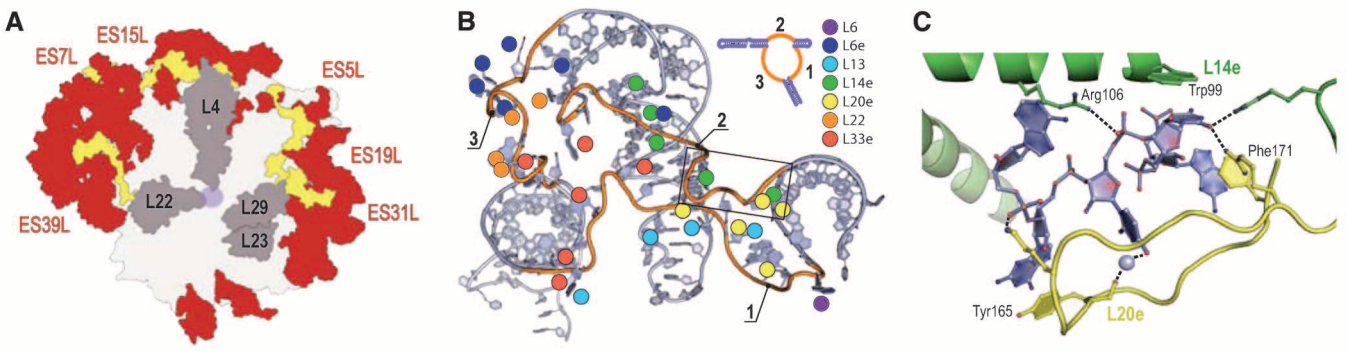

Fig. 3. Features of the rRNA expansion segments. (**A**) Extensions (in yellow) of conserved exit tunnel proteins (gray) associate with rRNA expansion segments (red). View of 60*S* is as in Fig. 2B, with the position of the exit tunnel rim represented by a purple circle near the center. (**B**) The structure of ES39L, colored according to its two-dimensional diagram (upper right), shows irregular single-stranded rRNA elements (orange) and indicates residues within these stretches whose exposed bases form interactions with surrounding proteins (circles colored according to interacting protein). A rectangular frame is drawn around the segment shown in (C). (**C**) Multiple interactions between proteins and a single-stranded rRNA stretch. A short fragment of ES39L (blue) interacts with L20e and L14e. Protein residues that stack with exposed bases are labeled; hydrogen bonds are represented by dotted lines.

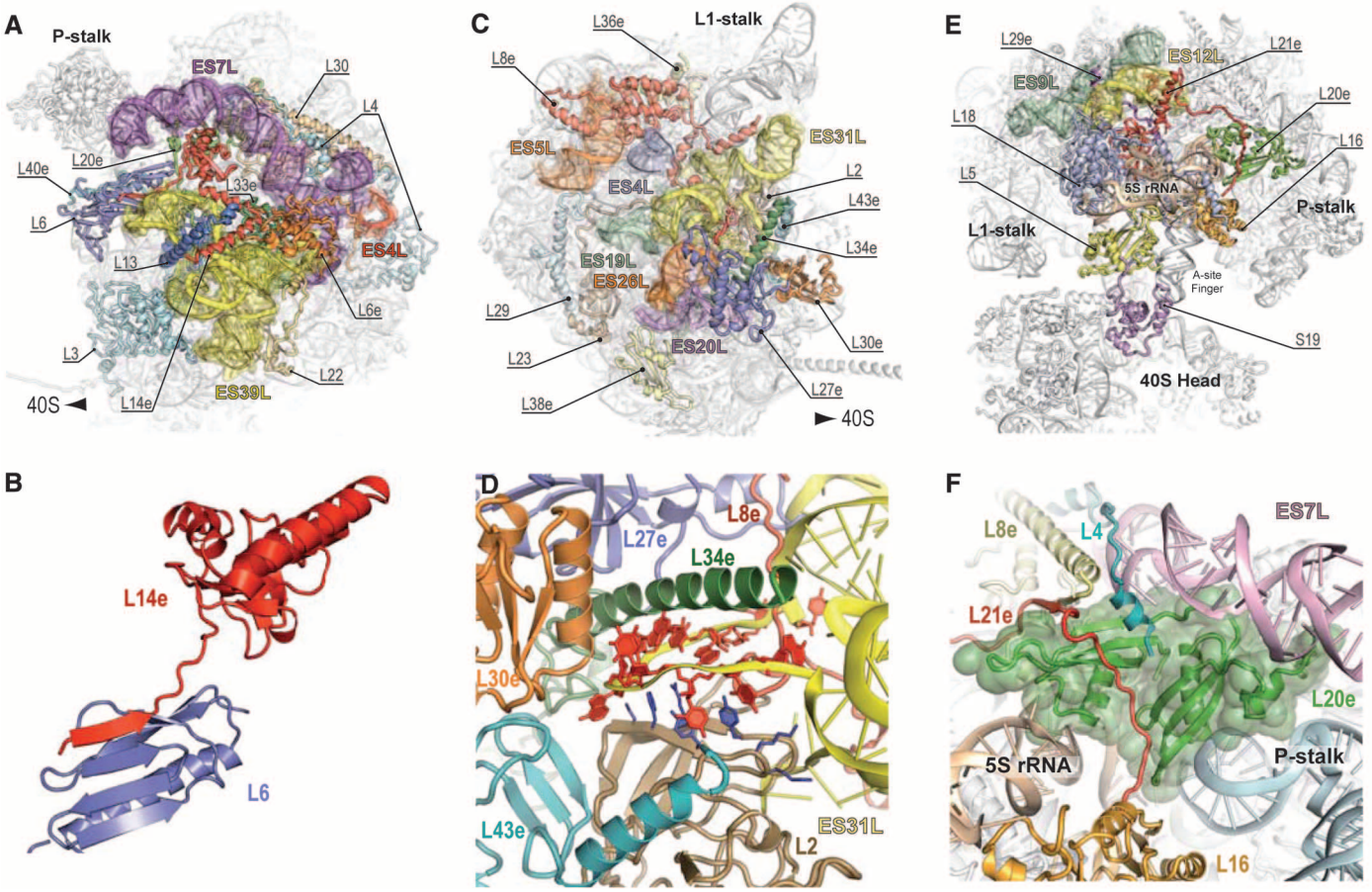

Fig. 4. Concentrations of eukaryote-specific elements along the 60*S* ring. (**A** and **B**) The back of the P stalk: (A) overview; (B) interprotein β sheet between the conserved L6 and the eukaryote-specific L14e. (**C** and **D**) The back of the L1 stalk: (C) overview; (D) the single-stranded stretch of ES31L (red) as a platform for protein-RNA interactions. Side chains of a structurally conserved domain in L2 that bind the eukaryotic rRNA element are depicted in blue. There are considerable differences in the sequence of this domain between yeast and bacteria. Evolution of conserved domains, as illustrated here, might result from the addition of eukaryote-specific elements. (**E** and **F**) The central protuberance region: (E) top view; (F) L20e forms multiple interactions with RNA and proteins.

structural role, in addition to transmitting information between the subunits and helping to coordinate their activities. The interaction surface between the two subunits is nearly doubled in eukaryotes because of the formation of additional bridges (Fig. 5A). In virtually all the added bridges, nearly all the participating components on both subunits are eukaryote-specific. Proteins play the dominant role in forming the eukaryote-specific bridges, in sharp contrast to bacteria (*26*). We describe here the molecular details of all major eukaryote-specific bridges (Fig. 5, figs. S13 and S14, and table S5).

Bridge eB8 is constructed by the eukaryote-specific protein S1e, which defines the far end of the 40*S* platform and ES31L (Fig. 5, B and C). In ribosome A, the bridge is formed via long-range interactions that are mediated by either positive ions or water molecules positioned between aspartates of S1e and phosphate groups of ES31L. The eukaryote-specific bridges are located at the periphery of the ribosome, where rotation of the small subunit results in large shifts. Hence, adaptation of the bridges to different states of the ribosome requires considerable structural plasticity of their components, as illustrated here by ES31L (Fig. 5B).

Just as the 60*S* component of bridge eB8, namely ES31L, is structurally linked to functionally important domains (Fig. 4C), so are

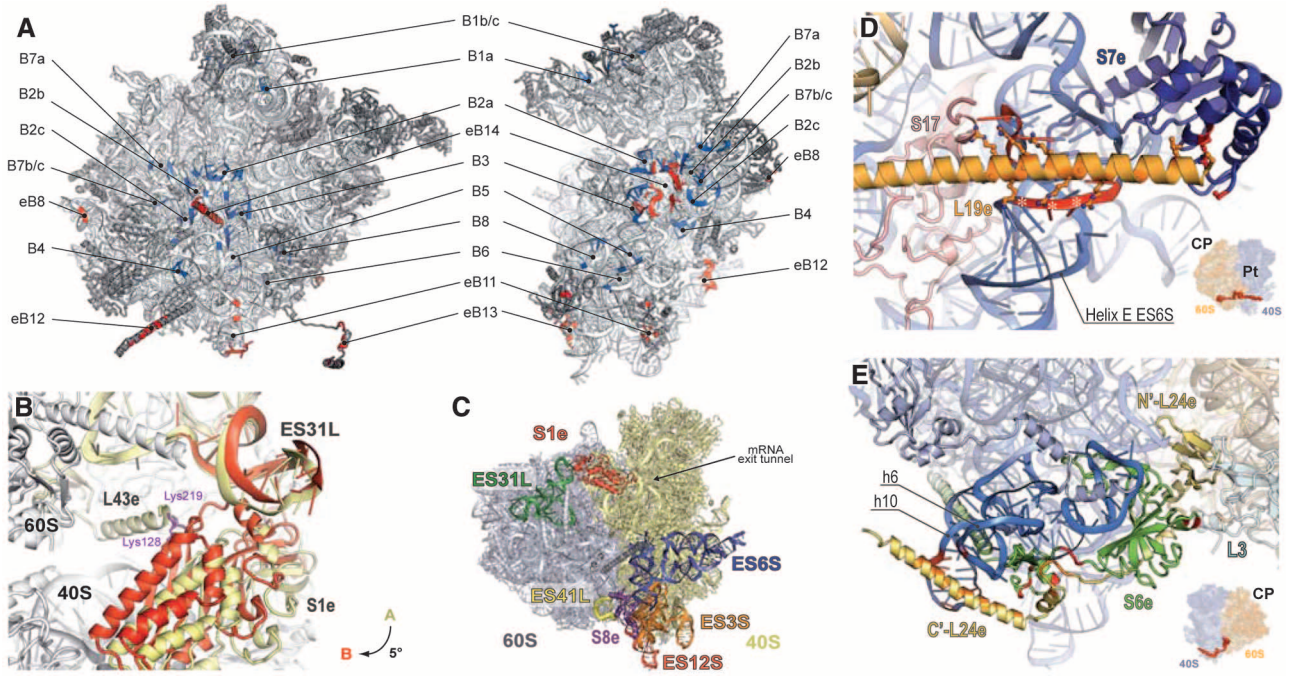

Fig. 5. Intersubunit bridges. (**A**) Interface view showing residues forming eukaryote-specific bridges (red) and conserved ones (blue). (**B**) Rearrangement of bridge eB8, showing the bridge in ribosome A (yellow) compared to that in ribosome B (red). (**C**) The location of bridge eB8 in proximity to the mRNA exit tunnel (arrow) and the location of bridge eB11 within a continuum of eukaryote-specific elements at the bottom of 80*S*. (**D**) Protein L19e is involved in forming bridge eB12. Residues of L19e that contact ES6S are shown as sticks. Asterisks (along red ribbon) highlight ES6S residues in proximity to the eIF4G binding site (*29*). (**E**) L24e extends from the 60*S* body to interact with S6e on the small subunit. In (D) and (E), rRNA and protein residues involved in forming the bridges are in red and orange in 40*S* and 60*S*, respectively. Lower right corners show locations of the corresponding bridges within 80*S*.

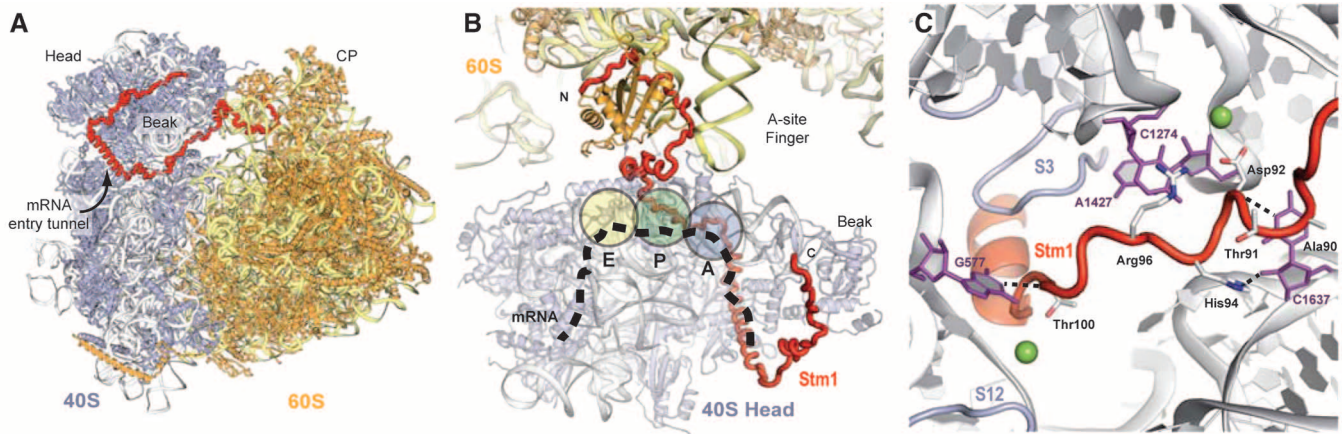

Fig. 6. Stm1 interacts with both subunits and prevents mRNA binding. (**A**) Stm1 (red) binds to 40*S* (blue) and 60*S* (yellow). (**B**) Top view of the 40*S* head and the CP of 60*S*, showing how Stm1 follows the mRNA pathway until the P site. Dashed black line represents the path of mRNA according to crystal structures of bacterial ribosomes (*38*). Rough locations of A-, P-, and E-tRNA sites are indicated. (**C**) Stm1 interacts with conserved rRNA residues (magenta) that bind mRNA or tRNA in functional complexes.

components on the 40*S* side. Protein S1e interacts directly with h26, S11, and S26e, which form part of the mRNA exit tunnel (Fig. 1 and Fig. 5C). Furthermore, cross-linking experiments resolved interactions between hepatitis C virus (HCV) internal ribosome entry sites (IRES) and protein S1e (*27*). Indeed, docking our 80*S* model into cryo-EM maps of the HCV IRES attached to human ribosomes (*28*) reveals that one of its contact sites on the ribosome is established by protein S1e.

Protein S8e is sandwiched between ES3S on the small subunit and ES41L on the large subunit, thus creating bridge eB11 (Fig. 5C and fig. S13). ES3S is part of the expanded network of interaction at the bottom of the small subunit that includes ES6S, making S8e a link in a large continuum of eukaryote-specific elements, ~100 Å in length, that begins on the platform of the small subunit, just below the mRNA exit tunnel where ES6S emerges (Fig. 5C).

The only eukaryote-specific bridge positioned at the center of the ribosome is bridge eB14 (fig. S14). The bridge is formed by protein L41e, which consists of a single α helix that is enveloped by conserved core rRNA. L41e protrudes from 60*S* into a binding pocket in the small subunit, which is lined by helices h27, h45, and h44, in proximity to the decoding center. Curiously, in the context of the full ribosome, L41e is much more strongly associated with 40*S* than with 60*S*.

Bridges contacting 40*S* from the side. A distinctive feature of the eukaryotic large subunit is two long protein helices extending from its left and right sides. These helices—eukaryote-specific additions to proteins L19e and L24e—create two bridges, eB12 and eB13 respectively, that are not buried within the intersubunit interface and are accessible from the solvent.

Bridge eB12 appearing below the mRNA exit tunnel is mainly formed through multiple interactions between several turns of the C-terminal α helix of L19e and the base of helix E in ES6S (Fig. 5D). The major part of the small-subunit side of this bridge is established by ES6S residues that were shown to lie in close proximity to the binding site for eIF4G, a protein that plays a central role in assembling the pre-initiation complex (*29*). This suggests involvement of eB12 and L19e in the last stages of translation initiation, in particular, subunit joining and shedding/releasing factors.

Protein L24e consists of an N-terminal domain that resides in 60*S*, followed by a long flexible linker that protrudes deep into the side of the 40*S* body and a C-terminal domain that reaches the back of 40*S* (Fig. 5E). The strong interactions of the C-terminal part of L24e with S6e and h10 constitute the bulk of bridge eB13. Comparison of ribosomes A and B suggests that the L24e C-terminal domain follows the movements of 40*S*, a feature facilitated by the protein's flexible linker, as if it were a bona fide 40*S* component. This architecture of L24e should be considered in light of the finding that L24e is a key player in translation re-initiation of polycistronic mRNAs and that its C-terminal domain mediates retention of eIF3 on the ribosome, a necessary condition for re-initiation (*30*–*32*).

The C-terminal helix of S6e harbors serines phosphorylated by S6K1 of the TOR pathway (*33*) and reaches the vicinity of ES6S helix B on the back of 40*S* (fig. S15). Taking into account the fact that we are missing the last 10 residues of the S6e C terminus, the structure raises the possibility that S6e interacts with factors that dock on ES6S or are involved in initiation or re-initiation.

Stm1. Previous studies have shown that protein Stm1 can associate with full ribosomes and inhibit translation, but the nature and role of these interactions was unknown (*34*, *35*). We find that Stm1 binds the head domain of 40*S* and precludes mRNA access by inserting an α helix through the mRNA entry tunnel (Fig. 6A). Furthermore, Stm1 follows the path of mRNA until the P site, contacting conserved residues from the 40*S* body that play a role in binding mRNA or tRNA at the P and A sites of functional ribosome complexes (Fig. 6, B and C). The protein then crosses to the 60*S* through interactions mainly with helix H84 and eventually exits 60*S* between 5*S* rRNA and protein L5 (Fig. 6A). Along its long path, Stm1 contacts nine different ribosomal proteins—one on 60*S*, eight on 40*S*. This conformation of Stm1 clamps the two subunits, prevents their dissociation, and further inhibits translation by excluding mRNA binding. Stm1 was shown to play an important role in yeast recovery after experiencing long periods of nutrient-deficient conditions. Because we purified our ribosomes from yeast grown for a few minutes under glucose starvation conditions (*9*), we suggest that either Stm1 binding or a conformational change of an already bound Stm1 are induced by such stress. Stm1 might act to preserve ribosomes and inhibit their activity until nutrients are abundant. It is thus a functional analog of prokaryotic and chloroplast stress-induced ribosome preservation proteins (*36*, *37*).

Conclusion. The model presented here provides a molecular description of the complete eukaryotic ribosome. It forms a framework for the design and analysis of further experiments that will shed light on diverse aspects of ribosome function, regulation, and assembly as well as the role of its eukaryote-specific elements.

References and Notes

1. T. M. Schmeing, V. Ramakrishnan, *Nature* **461**, 1234 (2009).
2. R. J. Jackson, C. U. Hellen, T. V. Pestova, *Nat. Rev. Mol. Cell Biol.* **11**, 113 (2010).
3. N. Sonenberg, A. G. Hinnebusch, *Cell* **136**, 731 (2009).
4. C. M. Spahn *et al.*, *Cell* **107**, 373 (2001).
5. O. Lecompte, R. Ripp, J. C. Thierry, D. Moras, O. Poch, *Nucleic Acids Res.* **30**, 5382 (2002).
6. M. Schüler *et al.*, *Nat. Struct. Mol. Biol.* **13**, 1092 (2006).
7. D. J. Taylor *et al.*, *Structure* **17**, 1591 (2009).
8. T. Becker *et al.*, *Science* **326**, 1369 (2009); 10.1126/science.1178535.
9. A. Ben-Shem, L. Jenner, G. Yusupova, M. Yusupov, *Science* **330**, 1203 (2010).
10. J. Rabl, M. Leibundgut, S. F. Ataide, A. Haag, N. Ban, *Science* **331**, 730 (2011); 10.1126/science.1198308.
11. See supporting material on *Science* Online.
12. W. Zhang, J. A. Dunkle, J. H. D. Cate, *Science* **325**, 1014 (2009).
13. P. Nissen, J. Hansen, N. Ban, P. B. Moore, T. A. Steitz, *Science* **289**, 920 (2000).
14. B. T. Wimberly *et al.*, *Nature* **407**, 327 (2000).
15. N. Ban, P. Nissen, J. Hansen, P. B. Moore, T. A. Steitz, *Science* **289**, 905 (2000).
16. D. A. Pomeranz Krummel, C. Oubridge, A. K. Leung, J. Li, K. Nagai, *Nature* **458**, 475 (2009).
17. M. Halic *et al.*, *Nature* **427**, 808 (2004).
18. K. Bokov, S. V. Steinberg, *Nature* **457**, 977 (2009).
19. P. Nissen, J. A. Ippolito, N. Ban, P. B. Moore, T. A. Steitz, *Proc. Natl. Acad. Sci. U.S.A.* **98**, 4899 (2001).
20. M. Diaconu *et al.*, *Cell* **121**, 991 (2005).
21. A. Meskauskas, J. D. Dinman, *Mol. Cell* **25**, 877 (2007).
22. C. M. Spahn *et al.*, *EMBO J.* **23**, 1008 (2004).
23. A. Korostelev, D. N. Ermolenko, H. F. Noller, *Curr. Opin. Chem. Biol.* **12**, 674 (2008).
24. M. H. Rhodin, J. D. Dinman, *PLoS One* **6**, e20048 (2011).
25. M. W. Smith, A. Meskauskas, P. Wang, P. V. Sergiev, J. D. Dinman, *Mol. Cell. Biol.* **21**, 8264 (2001).
26. M. M. Yusupov *et al.*, *Science* **292**, 883 (2001); 10.1126/science.1060089.
27. E. Babaylova *et al.*, *Nucleic Acids Res.* **37**, 1141 (2009).
28. D. Boehringer, R. Thermann, A. Ostareck-Lederer, J. D. Lewis, H. Stark, *Structure* **13**, 1695 (2005).
29. Y. Yu, I. S. Abaeva, A. Marintchev, T. V. Pestova, C. U. Hellen, *Nucleic Acids Res.* **39**, 4851 (2011).
30. H. S. Park, A. Himmelbach, K. S. Browning, T. Hohn, L. A. Ryabova, *Cell* **106**, 723 (2001).
31. T. Nishimura, T. Wada, K. T. Yamamoto, K. Okada, *Plant Cell* **17**, 2940 (2005).
32. O. Thiébeauld *et al.*, *EMBO J.* **28**, 3171 (2009).
33. I. Ruvinsky, O. Meyuhas, *Trends Biochem. Sci.* **31**, 342 (2006).
34. N. Van Dyke, J. Baby, M. W. Van Dyke, *J. Mol. Biol.* **358**, 1023 (2006).
35. V. Balagopal, R. Parker, *RNA* **17**, 835 (2011).
36. A. Vila-Sanjurjo, B. S. Schuwirth, C. W. Hau, J. H. Cate, *Nat. Struct. Mol. Biol.* **11**, 1054 (2004).
37. M. R. Sharma *et al.*, *J. Biol. Chem.* **285**, 4006 (2010).
38. L. B. Jenner, N. Demeshkina, G. Yusupova, M. Yusupov, *Nat. Struct. Mol. Biol.* **17**, 555 (2010).

Acknowledgments: We thank C. Schulze-Briese, M. Mueller, and the staff at the Swiss Light Source for advice on data collection strategy; K. Diederichs for guidance on estimating data quality; B. Seraphin and A. Urzhumtsev for invaluable discussions; M. Fournier and V. Chavant for performing mass spectrometry analysis; and S. Uge for assistance with computer facilities. Supported by a European Molecular Biology Organization long-term fellowship (A.B.-S.), the Human Frontier Science Program, French National Research Agency grants ANR BLAN07-3_190451 and ANR-07-PCVI-0015-01, and the European Commission SPINE2. Coordinates and structure factors have been deposited in the Protein Data Bank with accession codes 3U5B, 3U5C, 3U5D, 3U5E, 3U5F, 3U5G, 3U5H, and 3U5I.

Supporting Online Material

www.sciencemag.org/cgi/content/full/science.1212642/DC1
Materials and Methods
Figs. S1 to S15
Tables S1 to S5
References (*39*–*59*)

15 August 2011; accepted 4 November 2011
Published online 17 November 2011;
10.1126/science.1212642

The Structure of the Eukaryotic Ribosome at 3.0 Å Resolution

Adam Ben-Shem, Nicolas Garreau de Loubresse, Sergey Melnikov, Lasse Jenner, Gulnara Yusupova and Marat Yusupov

Science **334** (6062), 1524-1529.
DOI: 10.1126/science.1212642originally published online November 17, 2011